High temperature corrosion resistance of FeCr(Ni, Al) alloys as bulk/overlay weld coatings in the presence of KCl at 600 °C

Corrosion Science 213 (2023) 110896

Contents lists available at ScienceDirect

Corrosion Science

journal homepage: www.elsevier.com/locate/corsci

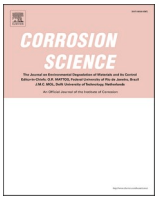

High temperature corrosion resistance of FeCr(Ni, Al) alloys as bulk/overlay weld coatings in the presence of KCl at 600 °C

Vicent Ssenteza *, Johan Eklund, Imran Hanif, Jesper Liske, Torbjörn Jonsson

Chalmers University of Technology, Gothenburg, Sweden

ARTICLE INFO

Keywords:
Biomass
High-temperature corrosion
Overlay weld
Breakaway oxidation

ABSTRACT

The long-term high temperature corrosion behavior of FeCr(Ni, Al) alloys, both in bulk form and as overlay welds, was investigated in a new experimental setup, in the presence of KCl at 600 °C. All the alloys experienced breakaway oxidation, with the bulk materials exhibiting better corrosion resistance than the overlay weld coatings with similar compositions. All results indicate diffusion-controlled kinetics, and the analysis revealed an improved corrosion behavior connected to an increased Cr content in the inward-growing scale.

1. Introduction

The selection of metallic materials for the superheaters for biomass- and waste-fired power plants is vital in enabling a good overall electrical efficiency of the plant. With electrical efficiency from biofuels in combined heat and power plants currently ranging from 25% to 37% [1], efforts are being made to improve the efficiency and economic feasibility of the power plants. The main challenge is the high temperature corrosion, that leads to rapid degradation of boiler components, e.g., causing tube failures and shortens tube lifetimes [2,3]. To limit high temperature corrosion, many boilers operate with steam temperatures below 450 °C [4]. The steam temperature may even be reduced further when combusting low-grade fuels due to their high impurity content which results in reduced electrical efficiency. The combustion of biomass and waste results in a flue gas containing corrosive species such as water vapor and alkali chlorides which have been shown to generate high corrosion rates for metallic components, e.g., superheater tubes, at high temperatures. It is well known that alkali salts lead to accelerated corrosion of superheater tubes by breaking down the protective oxide scale [2,5–15]. In particular, KCl has been shown to accelerate corrosion at high temperatures [9–12,14,15]. The accelerated corrosion of the superheater tubes thereby puts a strain on boiler performance.

Currently, low alloyed steels are the most used superheater materials due to their relatively low prices, even though they suffer rapid corrosion at the boiler temperature (around 500 °C) [16]. On the other hand, stainless steels offer an improved corrosion resistance that is attributed to their ability to form chromia (primary protection) in less aggressive environments in the relevant temperature span. However, in the environments found in biomass- and waste-fired boilers, the chromia scale formed by stainless steels has been shown to break down, leading to the formation of a poorly protective oxide scale (Fe-rich for Fe-based alloys) which initiates the process known as breakaway oxidation [7,17,18]. The reaction is fast, and the primary protection is usually broken down at an early stage of the operation, i.e the performance of the alloys relies on the protectiveness of the secondary protection oxide scale formed after breakaway oxidation. An alternative material class is the FeCrAl alloys, which may offer an improved primary protection by forming alumina at temperatures above 900 °C [19] due to its improved resistance to Cr-depleting species, such as alkali salts and water vapor. However, at the intermediate temperatures relevant for boiler operations, the formation of alumina has been reported to be very slow, providing a challenge for the use of FeCrAl alloys in these environments [20]. Ni-based alloys, e.g. A625, have also demonstrated promising corrosion resistance and have been used to mitigate corrosion attack in boiler components [21]. The Ni-based alloys in addition present with other benefits such as high strength and fabricability, which are desirable properties for application in harsh environment at high temperatures. However, the application of these Ni-based alloys is greatly limited by the high cost of Ni.

The selection of superheater materials for biomass- and waste fired boilers is limited due to the demand to have good mechanical properties as well as good corrosion resistance. Recent studies have shown that incorporating certain alloying elements, such as Cr, Al, Ni and Si, can improve corrosion resistance of bulk materials after breakaway oxidation [18,22,23]. On the other hand, the combination of high amounts of Cr, Al and Si has been shown to negatively affect the mechanical

* Correspondence to: Department of Chemistry and Chemical Engineering, Chalmers University of Technology, S-412 96 Gothenburg, Sweden.
E-mail address: ssenteza@chalmers.se (V. Ssenteza).

https://doi.org/10.1016/j.corsci.2022.110896
Received 8 July 2022; Received in revised form 5 October 2022; Accepted 1 December 2022
Available online 12 December 2022

properties. One solution which makes it possible to meet both requirements of the superheater material while also keeping down the cost is to apply a corrosion resistant coating (through e.g., overlay welding) to a material with good mechanical properties. However, more work is needed to understand how the corrosion properties is influenced by the chemical composition and how the corrosion resistance differs as bulk material or as overlay weld coating. In addition, since most research on the corrosion behavior of different alloys in harsh environments are focused on short-term behavior, long-term testing is needed in order to estimate the applicability of the observations in relation to the full-scale commercial application.

To understand the underlying corrosion mechanisms and determine the lifetime of key boiler components, systematic long-time exposures in relevant environments are needed. Currently, many of the laboratory methods deployed only offer the possibility to carry out short-term investigations with few samples. Spraying a known amount of KCl on samples [22] offers a controlled system but is only suitable for short-term exposures due to rapid evaporation of the salt at the present conditions. The use of salt pills [24] and continuous salt deposition [7] mimic full-scale commercial boiler, but present a less controlled system. To be able to carry out long-time investigations and be able to compare the performance of a larger number of samples under similar test conditions, it is necessary to develop a more robust and systematic method, in which KCl remains on the samples during long-time exposures and offers non-segregated corrosion attack for all the samples.

Thus, the aim of this study is twofold. Firstly, it is to develop an experimental setup for systematic long-term investigation of KCl-induced corrosion in laboratory where salt remains on the surface of the samples during long exposures giving similar conditions for many samples at the same time. Secondly, it is to implement the setup and investigate high temperature corrosion resistance of FeCr(Ni,Al) alloys in both bulk and overlay weld in presence of KCl at 600 °C.

2. Experimental procedure

2.1. Sample preparation

The alloys used in this study are presented in Table 1. The alloys were both bulk form and applied as overlay-welded coatings. The materials and coatings studied belong to different steel classes. A newly developed martensitic stainless steel SVM12, supplied by Vallourec S.A, acted as reference material. The rest of the materials were supplied by Kanthal AB. The bulk materials were received as coupons with the dimensions 20 × 10 × 2 mm. Overlay-welded coatings were produced by applying the alloys on a SVM12 substrate using the Mech-MIG with Pulse Multi Control technique to produce samples with the dimensions 20 × 10 × 4 mm. The coatings were applied on one of the faces of the SVM12 substrate and the rest of the sides were covered by a slurry coating to limit corrosion. SVM12 was used as the substrate for the overlay welded materials due to its good mechanical properties such as creep, rapture strength and toughness [25].

The edges of all the bulk materials were manually ground with 500 grit SiC while the flat surfaces were ground with P500 and P800 SiC paper using a grinding/polishing machine from Struers. The samples were then cleaned with acetone in an ultra-sonic bath and finally with ethanol. No sample preparation was performed on the coatings.

Table 1
Chemical composition (at%) of the different alloys used in this study.

Alloy	Cr	Al	Si	Mo	Mn	Ni	C	Fe
SVM12	10.9		1.01	0.3	0.69	0.32	0.63	Bal
Kanthal EF101	10.77	6.19	2.01		0.08		0.08	Bal
Kanthal EF100	9.00	6.87	0.50		0.17	0.39	0.07	Bal
Kanthal APMT	21.15	9.70	1.31	1.64	0.38		0.35	Bal
A625	24.16	0.42	0.43	5.61	0.38	64.22	0.50	4.29

2.2. Exposure setup

Fig. 1 shows a schematic drawing of the experimental setup. The setup parameters needed to be optimized to limit the KCl evaporation from the sample surfaces so that the salt remain during the entire long-term exposures. Two gas flow rates (0.5 cm/s and 0.1 cm/s) were investigated. The possibility to reduce the conversion of KCl(s) to KCl(g) on sample surfaces was also investigated by introducing KCl salt in an alumina container upstream in order to saturate the incoming gas with KCl (g). The gas composition in the furnace consisted of 5% O_2 + 20% H_2O and balanced by N_2. The temperature was set to 600 °C for both the samples and the KCl container. The equilibrium vapor pressure (EVP) of KCl at the set temperature was 3.4 ppm (calculated using FactSage 7.2 software (Fact PS database)). A temperature range of 597–603 °C with corresponding KCl EVP of 3.05–3.73 ppm, respectively, was considered.

To study the evaporation rate of KCl under different gas flows, three 24-carat gold coupons with areas 169 mm^2, 201 mm^2, and 199 mm^2 were used. The gold coupons were chosen as they are inert to the species present during the exposure. KCl was deposited on the gold coupons by spraying a solution consisting of 80 vol% ethanol with 20 vol% distilled water saturated with KCl while warm air passed over them to speed up the drying process. The coupons were weighed before and after salt deposition using a Mettler Toledo balance (model XP26), with a 6 decimal accuracy. The samples were then left to dry in a desiccator for 24 h and weighed right before exposure. The samples were mounted horizontally on an alumina sample holder and exposed for 2 h and 24 h.

To examine the robustness of the optimized setup, 18 SVM12 (reference material) coupons were sprayed with KCl salt in the range of 0.2–0.7 mg/cm^2 and exposed for 168 h. The samples were mounted vertically on alumina sample holders and placed at different locations in the heating zones of a horizontal silica tube furnace.

2.3. Furnace exposures

Several exposures were performed on the bulk materials and overlay weld coatings using the setup described in previous section. Firstly, a 500-hour exposure was performed where the samples were sprayed with 0.5 mg/cm^2 of KCl. Thereafter, a series of exposures (168, 500, 1000, 2000 and 8000 h) were performed where the samples were sprayed with 2 mg/cm^2 of KCl. The amount of KCl salt sprayed on the samples was calculated based on the salt evaporation rate from the KCl evaporation test. All the exposures were performed in an environment consisting of 5% O_2 + 20% H_2O + N_2 (Bal) at 600 °C with a KCl container upstream samples (see Fig. 1).

2.4. Analysis

The exposed samples were analyzed with scanning electron microscope (SEM) to investigate the extent of the corrosion attack and the microstructure of the corrosion products. Cross-sections of the exposed samples were prepared by first sputtering a thin layer of gold on top of the oxide to make it easy to distinguish the surface of the oxide during analysis. A thin silicon wafer was glued on one of the samples surfaces and was left to dry for 24 h. The samples were then cut using a low-speed diamond saw. Due to the uneven surface of the coatings, the samples were casted in epoxy resin to protect the oxide scale. The cast samples were cut using a high-speed aluminum oxide saw and the cross-sections mechanically polished with 4000 grit SiC. The polished cross-sections were ion milled using a Gatan PECS II broad ion beam (BIB) milling system operated at 6 kV for 0.5–2 h and a Leica TIC3X milling system operated at 8 kV for 4–6 h.

The prepared cross sections were analyzed using a FEI Quanta 200, operated at an accelerating voltage of 10–20 kV in high vacuum mode. Imaging was performed using backscattered electrons (BSE). Chemical

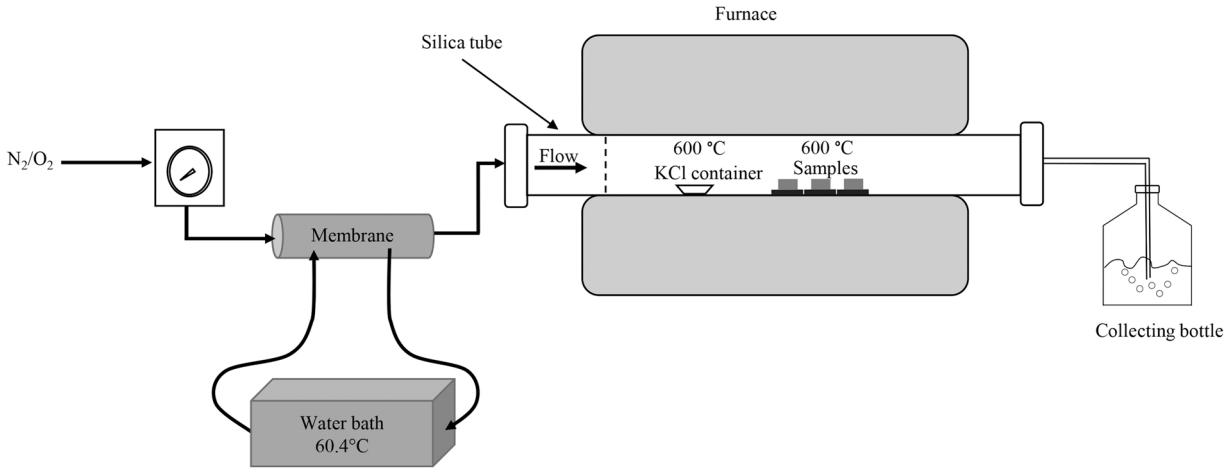

Fig. 1. Schematic drawing of experimental setup showing different parts and sample positions.

analysis was performed using an Oxford Instruments X-MaxN 80 T EDX connected to the SEM. Furthermore, X-ray diffraction was performed on samples using a D8 advance diffractometer from Bruker with measured angle range of $10° < 2\theta < 90°$ to determine the crystalline oxide phases.

3. Results

3.1. KCl evaporation on gold samples

The aim with the exposures was to simulate a corrosive environment in a biomass/waste-fired boiler in which KCl is known to be one of the main corrosive species. To be able to perform a long-time exposure with KCl remaining on the sample surface, a better understanding of the KCl evaporation and how it is affected by the flow rate and the presence of KCl(g) in the setup is needed. In the test of 0.5 cm/s without the KCl container, 87% (0.31 mg/cm^2) of all the sprayed KCl was evaporated from the gold samples after 24 h. For the test of 0.5 cm/s with KCl container, 0.17 mg/cm^2 salt was evaporated, which correspond to 68% of the KCl sprayed before exposure. In the test of 0.1 cm/s with KCl container, approximately 0.07 mg/cm^2 of the salt was evaporated, which correspond to about 7% of the salt sprayed.

The initiation of the evaporation was in addition investigated in order to measure KCl evaporation during the first hours of exposure. In a 2-hour test where a flow of 0.1 cm/s with KCl container was investigated, about 0.02 mg/cm^2 of salt had evaporated, which indicated a faster initial evaporation rate within the first hours of exposure (see Fig. 2).

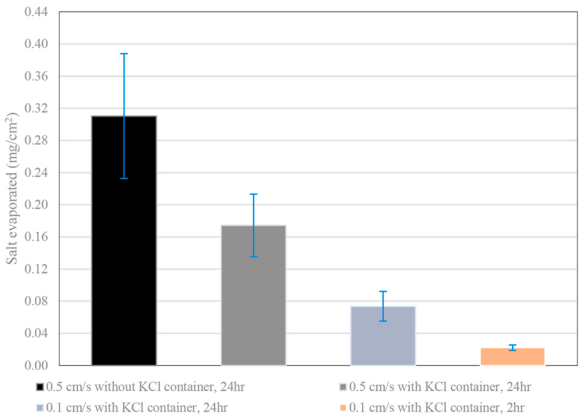

Fig. 2. Amount of KCl salt evaporated after 24 h respective 2 h on gold samples.

3.2. Influence of sample position

The impact of sample position/variation of KCl(s) within the furnace was investigated by exposing 18 martensitic SVM12 samples. The position as well as the amount of deposited KCl (in the range of 0.2–0.7 mg/cm^2) was registered for each sample. Fig. 3 shows the mass gain recorded for the 18 samples exposed in 5% O_2 + 20% H_2O + N_2 (Bal) at 600 °C for 168 h in the presence of pre-deposited KCl and KCl container upstream the samples. All samples exhibited mass gain in the same range (between 4.7 mg/cm^2 and 6.8 mg/cm^2) regardless of the different position in the furnace. However, some samples showed signs of spallation as the samples cooled down after the exposure. Samples that experienced spallation are marked with an asterisk symbol. The amount of KCl sprayed on the samples also showed no direct impact on the mass change of the SVM12 samples, e.g., samples 3, 7 and 16 sprayed with 0.5, 0.3 and 0.2 mg/cm^2 had mass gains of 5.0, 6.8 and 6.3 mg/cm^2 respectively.

3.3. Oxide microstructure bulk/overlay weld coatings

The exposure setup was used in order to investigate the corrosion resistance of different FeCr(Ni, Al) alloys as well as the difference in performance between bulk materials and the overlay weld coatings for each composition. Exposures were performed for 500 h in 5% O_2 + 20%

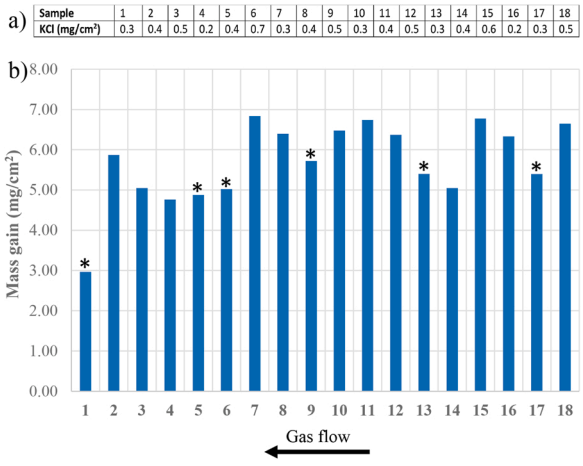

Fig. 3. Amount of KCl deposited mass gain and sample positions for the 18 SVM12 samples (reference material) exposed in 5% O_2 + 20% H_2O + N_2 (bal) at 600 °C for 168 h. Influence of sample position in the furnace on the corrosion attack. * Indicate samples that experienced oxide spallation after exposure.

$H_2O + N_2$ (Bal) with 0.5 mg/cm^2 KCl and a KCl salt container upstream as well as 168 h, 500 h, 1000 h, 2000 h and 8000 h in 5% O_2 + 20% H_2O + N_2 (Bal) with 2.0 mg/cm^2 KCl and a KCl salt container upstream at 600 °C.

The samples sprayed with 0.5 mg/cm^2 KCl and exposed for 500 h were selected for the microstructural investigation. They showed the same general corrosion trend and microstructure as all the different exposure times. In addition, all oxide features were easier to identify with SEM/EDX after 500 h than for the 168 h, while the challenge with scale spallation during cooling and cross section preparation was smaller than for the longer exposures. The measured oxide scale showed that all the exposed samples quickly experienced breakaway corrosion, i.e., after less than 168 h. The scale thickness measurements from all the investigated exposure durations showed the same trend between the different materials and coatings, see measured oxide thickness in Fig. 4. It may be noted that some samples experienced spallation in some regions. However, the measured thickness is focused on regions without spallation and the spread represents local differences in oxide scale thickness.

3.3.1. Reference material (SVM12)

Fig. 5 shows an SEM-BSE image of an ion milled cross section displaying the corrosion products formed on SVM12 as well as the alloy beneath the corrosion layer after exposure for 500 h in 5% O_2 + 20% H_2O + N_2 (Bal) at 600 °C with 0.5 mg/cm^2 KCl. Unreacted KCl particles could be observed on top of the oxide scale. This was confirmed using SEM/EDX point analysis and is in good agreement with the setup measurements, the calculations based on KCl evaporation as well as the XRD results. The alloy formed a thick oxide scale (measured thickness in the range of 120–130 μm) that could be divided into two layers; an outward growing almost pure Fe-oxide layer (about 60–76 μm in thickness) and an inward growing layer (interpreted as a mixed-spinel) with a thickness of about 32–54 μm. The microstructural investigation indicated that the outward growing layer could be divided into different Fe-oxide layers, i.e., 16 μm thick hematite layer above a magnetite layer. This was concluded by observing the oxide grain size as well as the SEM/BSE contrast in combination with XRD.

The outward-growing layer was generally dense, with porosity in the middle regions (excluding the cracks induced by sample preparation). The inward growing layer was dense close to the outward-growing scale but more porous at the bottom part. The inward-growing layer consisted of approximately (35 at% Cr, 60 at% Fe, 3 at% Si, cations) and was interpreted as a spinel oxide. The region at the bottom had been shattered during sample preparation. W-rich particles were observed as bright-contrast particles in the spinel and were confirmed using SEM/EDX point analysis. Traces of Cl (less than 1% at) were detected in the metal/oxide interface in some regions.

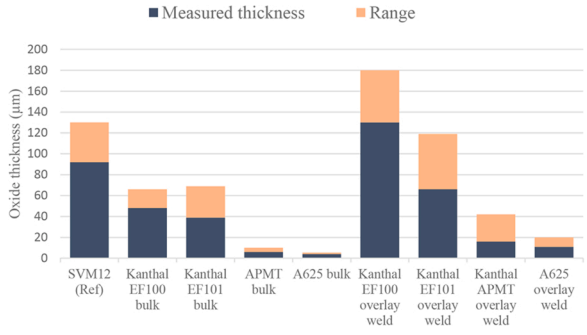

Fig. 4. Measure oxide thickness and calculated oxide thickness of alloys exposed in 5% O_2 + 20% H_2O + N_2 (Bal.) at 600 °C for 500 h in presence of 0.5 mg/cm^2 KCl (s) and KCl container.

3.3.2. Bulk material and overlay weld coatings

Fig. 6 shows SEM-BSE images of ion milled cross sections of all the alloys/coatings investigated in this study exposed in 5% O_2 + 20% H_2O + N_2 for 500 h in the presence of KCl (s). Generally, both the bulk materials and the overlay weld coatings formed thick oxide scales, see summary of measured thickness in Table 2. The bulk FeCrAl alloys (Kanthal® EF100, Kanthal® EF101 and APMT) displayed intermediate corrosion rate, with APMT having the thinnest oxide among them. All the oxide scale microstructures can be divided into an outward-growing layer and an inward-growing layer, similar to the SVM12 reference sample. The inward-growing layers in these cross-section images are colored to make them easy to observe. The outward/inward growing oxide interfaces are marked with a dashed line. All the analysis performed on composition of the oxides is presented in cations.

3.3.3. Bulk materials

Fig. 6a$_1$) shows a SEM/BSE cross section image of the oxide scale formed on Kanthal® EF100. The material formed a 48–66 μm thick duolayered oxide scale. The outward growing layer is dense and consisting of Fe-oxide with indications of hematite and magnetite, revealed by the darker contrast at the upper regions and bright contrast at the bottom regions. The inward-growing scale was homogenous and dense and interpreted as Fe-, Cr-, Al-spinel consisting of 55 at% Fe, 25 at% Cr and 20 at% Al. An approximately 9 μm deep nitridation zone (NZ) was observed underneath the oxide scale. Kanthal® EF101 with a similar composition as EF100 (except for difference in Si content) formed thinner oxide scale of about 39–69 μm, see Fig. 6b$_1$. The outward growing scale on EF101 was Fe-oxide while the inward-growing scale were dense and consisted of 35 at% Fe, 40 at% Cr and 20 at% Al with about 5 at% Si. Nitrogen and enrichments of aluminum were detected beneath both scales, indicating the formation of a nitridation zone to a depth of about 17 μm.

The microstructural investigation of APMT (Fig. 6c$_1$) showed that the material formed an about 10 μm thick oxide scale. The scale could again be divided into outward-growing and inward-growing scales with a similar thickness. The outward-growing layer was dense and Fe-rich with traces of Cr and Al close to the original metal interface, i.e the interface between the outward- and inward-growing scale. The inward-growing scale consisted of 15 at% Fe, 60 at% Cr, 20 at% Al, 2 at% Si and 3 at% Mo with porous darker regions close to the metal/oxide interface. The presence of Al and N was gain found below the oxide scale, indicating the formation of a 10 μm deep nitridation zone.

Alloy A625 (Fig. 6d$_1$) formed an oxide scale with a thickness of about 5.5 μm. The microstructural investigation showed that the oxide scale was undulating and covered by K_2CrO_4, confirmed by XRD and SEM/EDX point analysis. The oxide scale could again be divided into outward-growing and inward-growing oxide scale. The outward-growing scale was characterized by cracked oxide above a dense layer. The outer regions of the outward-growing oxide consisted of 40 at% Ni, 35 at% Cr and 20 at% Fe while the inner regions were Ni-rich oxide mixed with Cr and Fe (70 at% Ni, 20 at% Cr and 5 at% Fe). The inward-growing oxide layer was dense and was found to be enriched in Cr with a composition of about 70 at% Cr, 25 at% Ni and 3 at% Fe. Traces of Cl were detected throughout the oxide scale (below 1 at%). Smaller metal grains were observed about 4 μm below the metal/scale interface. This region was depleted in Cr and enriched in Ni (75 at% Ni and 20 at% Cr, 5 at% Mo).

3.3.4. Overlay weld coatings

The composition, oxide scale thickness and grain size of the overlay weld coatings were investigated with SEM/EDX. The investigation showed a homogenous thickness of the welds and a composition in the same range as the bulk material, see Table 2. It may be noted that a higher Fe content was detected in the Ni-based A625 overlay weld in comparison to the bulk version which is attributed to interdiffusion from the SVM12 substrate. In addition, the grain size was found to be larger for all of the overlay welded materials compared to bulk counterparts,

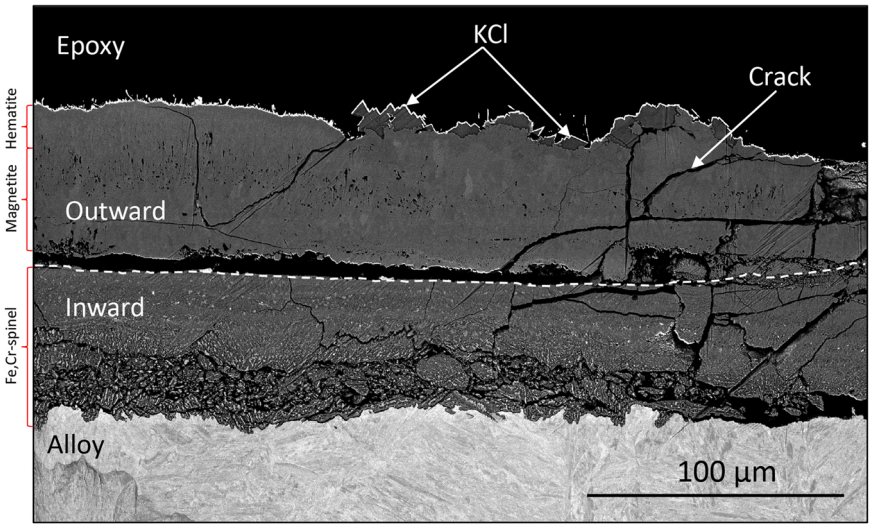

Fig. 5. SEM-BSE cross section of SVM12 after exposure in 5% O_2 + 20% H_2O + N_2 (Bal) for 500 h at 600 °C in presence of 0.5 mg/cm^2 KCl and KCl container in upstream.

compare e.g., Fig. 6b_1 and b_2.

The Kanthal® EF100 overlay weld coating (Fig. 6a_2) formed a 130–180 µm thick oxide scale. The outward-growing layer is porous and some of the scale spalled of. SEM/EDX analysis revealed that the chemical composition of the outward-growing layer was almost pure Fe-oxide. The inward-growing oxide layer was generally characterized by alloy grain boundary attacks (GBA) with a depth in the range of 75–108 µm. The oxide within the GBA has a darker contrast at the centers which were found to be enriched in Cr and Al (35 at% Cr, 30 at% Al and 35 at% Fe). The adjacent regions surrounding the GBA were found to be depleted in Cr and enriched in Fe (5 at% Cr, 10 at% Al and 85 at% Fe). Low levels of Cl (less than 1 at%) were detected in the inward growing oxide.

Kanthal® EF101 overlay weld coating (Fig. 6b_2) formed an oxide scale with a thickness in the range of 66–119 µm. The outward-growing layer was again identified as Fe-rich oxide. There were indications that the outward-growing Fe-oxide was multilayered consisting of hematite on top of magnetite. The outer part of the iron oxide was porous and was intermixed with K_2CrO_4. The inward-growing oxide layer was dense with some cracks (induced by sample preparation). SEM/EDX analysis revealed that this layer consisted of 50 at% Fe, 30 at% Cr and 15 at% Al, 5 at% Si. The lower regions of the inward growing scale were Cr-rich (40 at%). Below the scale, N and Al (enrichments) were detected indicating the formation of a nitridation zone (15 µm deep). In the bulk, below the scale/metal interface, zirconium precipitates were observed in the metal grain boundaries (bright particles in the BSE image).

The APMT overlay weld coating (Fig. 6c_2) formed an oxide scale with a thickness of 36–45 µm. It is worth noting that this sample suffered scale spallation and cracking, presumably during sample preparation. Large K_2CrO_4 particles were found on most parts of the investigated surface. The outward-growing layer is characterized by porosity and an undulating oxide surface. The microstructural investigation revealed that it consists of pure Fe-oxide. Traces of Cl were also detected in the outer parts of the scale close to the scale/gas interface. A large crack was observed between the outward- and inward-growing scales. It is possible that this is an artifact caused by sample preparation. The inward-growing scale is homogenous and consists of 50 at% Cr, 20 at% Al, 25 at% Fe, 5 at% Mo and 2 at% Si. Below the inward-growing scale, there were voids and some pores. A nitridation zone (about 38 µm) was observed below the scale. Mo-rich precipitates (bright regions in the BSE image) of about 1 µm were observed in the inward-growing scale and in the nitridation zone.

The A625 overlay weld coating (Fig. 6d_2) formed an oxide scale with a thickness of about 25–39 µm. It may be noted that the outer part of the oxide had been shattered during sample preparation. The outward-growing scale contained pores and was identified as Ni-rich oxide mixed with Fe (80 at% Ni, 15 at% Fe, 5 at% Cr). The outermost regions contained more Fe (about 20 at%). The inner regions of the outward-growing oxide contained larger pores. The inward-growing oxide was very thin layer (6–9 µm) and contained some pores. It consisted of a mixture of Cr, Ni, and Fe (30 at% Cr, 55 at% Ni and 10 at% Fe, 5 at% Mo). Within the alloy matrix, bright contrast spots were observed and identified as Mo-rich precipitates. Minor amount of Cl was detected throughout the scale (less than 1 at%).

4. Discussion

4.1. General remarks

In order to meet the demand to select materials and develop new materials/coatings for applications involving boiler environments, a combination of reliable laboratory investigations and tests in real boilers is needed. Investigations of the environment in commercial boilers have shown the presence of KCl(s)/KCl(g) in regions with high temperature corrosion challenges. The amount of potassium and chlorine in the flue gas depends on the fuel mix and position/temperature but has been reported to range from 0.033 to 1.66 wt% and 0.025–2 wt% [2] and as high as a potassium content up to 15–20 wt% and chlorine content up to 3–4 wt% [26]. It is a challenge to set up long-term laboratory exposures with a controlled gas flow and controlled amount of KCl(s) mimicking the KCl(s) found in deposits described above in the temperature range of 600 °C due to the rapid evaporation of KCl. In this study, the investigation of the KCl evaporation rate and the impact of flow rate as well as the results from the KCl(s)/KCl(g) furnace setup provide an environment where the amount of KCl(s) for long-term exposures could be set for a large number of samples in a system with a controlled gas flow, see Fig. 3. It should in this context be noted that unreacted KCl remains even after all long exposures independent of position and the impact of small deviations in the amount KCl is limited, see Fig. 3a and b.

The results from the long-term corrosion exposures of bulk materials and overlay weld coatings showed that the laboratory environment (O_2 + H_2O + N_2 + KCl(s)/KCl(g)) causes initially fast breakaway corrosion for all the samples as expected in this environment/temperature. This is in line with a breakaway mechanism where oxidation of stainless steels is accelerated due to formation of potassium chromate (observed on many samples in this study, see e.g. Fig. 6b_2, c_2, and d_1) and as reported

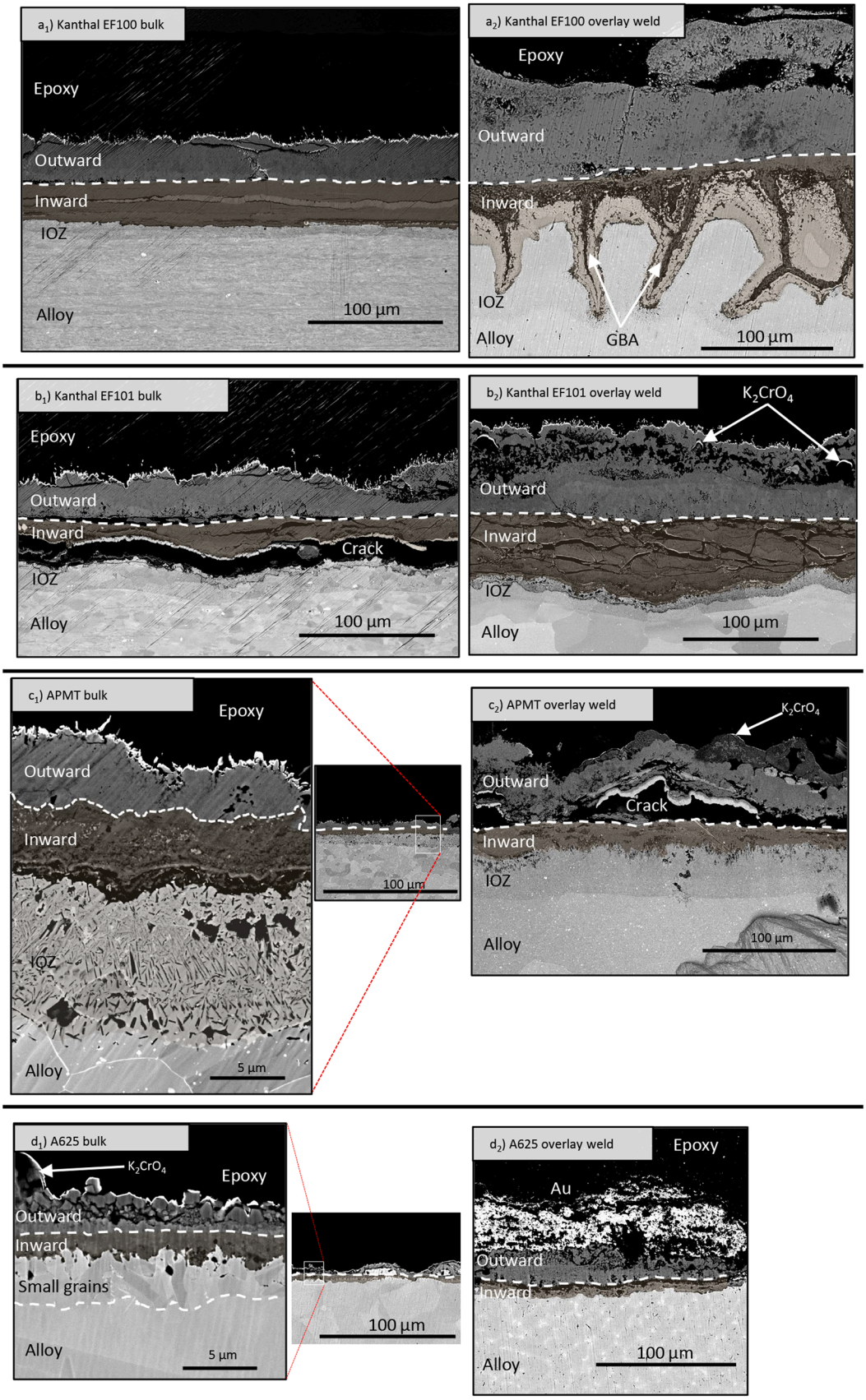

Fig. 6. SEM-BSE cross section of bulk materials and corresponding overlay weld after exposure in 5% O_2 + 20% H_2O + N_2 (Bal) for 500 h at 600 °C in presence of 0.5 mg/cm^2 KCl and KCl container upstream the samples. The inward-growing layers were colored to help in comparison between bulk materials and overlay weld coatings.

Table 2
Measure oxide thickness and calculated oxide thickness of alloys exposed in 5% O_2 + 20% H_2O + N_2 (Bal.) at 600 °C for 500 h in presence of 0.5 mg/cm_2 KCl (s) and KCl container upstream the samples.

Name of Alloy	Oxide thickness (μm)		
	Total thickness	Outward growing	Inward growing
SVM12 (Ref)	92–130	60–76	32–54
Kanthal EF100 bulk	48–66	29–33	19–33
Kanthal EF101 bulk	39–69	26–49	13–20
APMT bulk	6–10	3–5	3–5
A625 bulk	4–5.5	2.5–3.5	1.5–2
Kanthal EF100 overlay weld	130–180	55–72	75–108 (GBT)
Kanthal EF101 overlay weld	66–119	38–57	28–62
APMT overlay weld	42–45	25	17–20
A625 overlay weld	25–39	19–30	6–9

in previous studies [13,27,28]. Thus, the experimental setup provides a controlled corrosive environment with a very short incubation time to breakaway with KCl(s)/KCl(g) present throughout all the long exposures.

The characterization of the corrosion products was performed using SEM/EDX. The XRD was also used, however it was not possible to detect all the phases within the scales. Therefore, much of the XRD data was omitted for this work. Generally, the microstructural investigation revealed that the overlay weld coatings formed faster growing oxide scales than their corresponding bulk materials (see Table 2). This indicate that overlay welded coatings has a more vulnerable microstructure under exposure conditions containing KCl(s)/KCl(g). Despite the different growth kinetics, all the bulk material/coatings formed corrosion products could be divided into two layers, i.e., outward- and inward-growing oxide in accordance with previous studies where it has been shown that as the corrosion behavior transitions from the primary regime to the secondary regime, a diffusion-controlled growth of a multi-layered oxide scale [18,29]. The microstructure is in addition in line with what has been observed for exposed materials in commercial boilers burning straw [30], Refuse Derived Fuel [31] and waste [32]. The measured oxide thicknesses showed that the corrosion behavior exhibited by all the alloys followed a similar trend for all the exposure durations (168 h, 500 h, 1000 h, 2000 h and 8000 h) indicating different corrosion resistance in the secondary regime, i.e., behavior after breakaway oxidation on all alloys in presence of KCl(s)/KCl(g).

4.2. Experimental setup — long time exposures in the presence of KCl

Several different laboratory setups and techniques have been implemented to mimic and investigate the corrosiveness of biomass/waste fired boiler environment in the laboratory focusing on a simplified environment containing e.g., KCl(s)/KCl(g). These setups include e.g., spraying KCl solution on samples [22,27], depositing slurry [33], applying salt powder [34], condensation of KCl [7] and applying salt pills [24]. All laboratory investigations have shown that KCl(s)/KCl(g) is initially very corrosive towards steels and stainless steels at 600 °C, see e.g. [2,9,14,35]. However, long-time exposures with a controlled amount of KCl(s) in a controlled flow are rare. This is due to the relatively high evaporation rate of KCl observed at 600 °C.

The initial reaction routes for KCl(s) at the material surface may take two main directions, i.e., evaporation (Eq. (1)) or reacting with the chromium-rich corundum-type oxide (on stainless steels/FeCrAl alloys) in the primary protection to form potassium chromate (Eq. (2)) K_2CrO_4(s) and HCl(g) [36,37].

$$KCl(s) \rightarrow KCl(g) \quad (1)$$

$$Cr_2O_3(s) + KCl(s) + 2H_2O(g) + \tfrac{3}{2}O_2(g) \leftrightarrow 2K_2CrO_4(s) + 4HCl(g) \quad (2)$$

The setup in this study minimizes KCl(g) evaporation (Eq. (1)) over the samples due to a low flow rate and a source of KCl(s) upstream the samples, saturating the gas with KCl. The initiation and breakdown of the primary protection has been reported to be fast (less than 168 h for all alloys/coatings in this study). This results in limited amount of KCl reacting with the initial chromium-rich oxide in accordance with Eq. (2). The corrosion mode following breakaway will generate an iron/nickel-rich oxide scale in contact with the KCl(s) deposit. This stage (secondary regime) simulates a majority of the lifetime of a boiler component under a corrosive deposit. Thus, from a long-term corrosion perspective, it is important to know the rate at which KCl(s) evaporates in the laboratory setup and how it is dependent on the flow in order to be able to investigate the long-term corrosion behavior. In this study, KCl(s) was maintained on the samples surfaces during exposures by ensuring low evaporation of KCl and calculating the amount needed for the entire exposure. The exposures on a gold sample revealed the impact of flow rate on evaporation of KCl, i.e., 0.31 mg/cm^2 (87%) and 0.07 mg/cm^2 (68%) of the KCl evaporated with gas flow rates of 0.5 cm/s and 0.1 cm/s respectively after 24 h. The KCl(g) equilibrium partial pressure was calculated to be 3.4 ppm at 600 °C and the measured evaporation rate 0.01 mg/cm^2h are in line with the expected evaporation as well as earlier reported data [7,38]. In order to reduce the evaporation rate, large amounts of KCl(s) were introduced upstream the samples, see Fig. 1. This setup decreased the evaporation rate from 0.01 mg/cm^2h to 0.003 mg/cm^2h. However, it may be noted that the salt evaporation rate is not linear and initially faster, as seen from the 2-hour KCl evaporation test. This may be explained by an incubation time before the gas is saturated in KCl(g) and/or the morphology of the salt. The surface of the salt becomes smoother as smaller particles detach from edges (reducing dislocation concentration in the salt powder) to form surface mobile layers. Less edges and a reduced/absent thin KCl(s) layer may with time reduce the KCl evaporation rate [39]. However, the small difference would not have any large impact on the overall corrosion attack of the secondary protection.

Thus, the setup used in this study provides KCl(s) rich environment for a large set of samples in a controlled flow rate, regardless of their position in the furnace. In the reference exposure with the same material, all the samples exhibited mass gains in the same range (between 4.7 mg/cm^2 and 6.8 mg/cm^2). This is important for the evaluation of the corrosion behavior of different materials/coatings in the same exposure. The observed spread in mass gain of the reference material is interpreted to be caused by spallation of some samples as indicated in Fig. 3. Oxide spallation is a phenomenon that is well documented in both KCl-rich laboratory exposures e.g., [7] and in biomass/waste boiler exposures [31].

4.3. Corrosion resistance of bulk and coating materials

4.3.1. Reference material (SVM12) — impact of KCl(s)

Oxidation in 5% O_2 + 20% H_2O + N_2 (Bal) in presence of KCl(s)/KCl(g) resulted in rapid breakaway corrosion for the reference material SVM12 leading to formation of thick oxide, see Fig. 5. Alloys containing lower amounts of chromium, i.e., marginal chromia formers, tend to quickly transition into secondary protection when exposed to KCl(s) due to the low Cr-content/supply of Cr to the oxide scale. These alloys are not able to supply enough Cr to keep the protective primary scale in the present corrosive environments at intermediate temperatures (600 °C) and the oxide scale is instead transformed into a poor protective iron-rich scale [40–43]. The mechanisms involved have been shown to be the formation of chromium hydroxide ($CrO_2(OH)_2$) (in the presence of water vapor) or the formation of potassium chromate (K_2CrO_4) in the presence of alkali salts, which results into chromium depletion, consequently resulting in the formation of iron-rich oxide. Because of the low Cr content and little or no Al/Si, the results from the current study

indicate that SVM12 neither is able to develop a good secondary protection (reformation of a Cr/Al/Si-rich layer) after breakaway oxidation even after very long exposure times (8000 h).

Traces of Cl were detected across the oxide scale, which may influence the rate of propagation in accordance with the mechanism known as the 'chlorine cycle' [44]. However, the dense oxide microstructure as well as the oxidation kinetics (approximately parabolic) indicated diffusion-controlled kinetics and an electrochemical mechanism [45]. The diffusion of cations through the oxide has been reported to occur mainly via grain boundaries at 600 °C as reported by e.g., Töpfer et al. [46]. In the same study, the authors reported that the diffusivity of iron was higher than for other alloying elements such as chromium, aluminum, or nickel in the spinel phase (inward growing scale). This is in good agreement with observations made in the current study, in which the outward-growing oxide is iron oxide after all exposure times (up to 8000 h). The calculated parabolic rate constants (Kp values) indicate that the material exhibit a sub-parabolic behavior which may be explained by the expected grain growth in the iron oxide which has previously been shown to occur at 600 °C [47].

4.3.2. Corrosion resistance – bulk/overlay weld coatings

All the bulk/coatings exposed in 5% O_2 + 20% H_2O + N_2 in the presence of KCl(s)/KCl(g) experienced breakaway oxidation within the first 168 h of exposure, leading to the formation of Fe/Ni-rich oxides scales as seen in Table 2 (oxide thickness measurements) and Fig. 6 (cross-sections). However, the oxide growth kinetics varies for the different alloys following breakaway oxidation indicating different secondary protection for the bulk/overlay welds. Kanthal EF100 (Fig. 6a_1/a_2) exhibited similar corrosion behavior as the reference material (SVM12) while the rest of the alloys showed improved corrosion resistance, i.e., Kanthal EF101, APMT and A625, see Fig. 6b_1/b_2, c_1/c_2 and d_1/d_2 respectively.

4.3.3. Chemical composition – impact on secondary protection

SVM12 and Kanthal EF100 showed a very similar corrosion response, see Table 2 and compare Figs. 5 and 6a_1. This indicates that Kanthal EF100 is not able to reform a protective layer after breakaway oxidation. The microstructure investigation showed an improved corrosion resistance for Kanthal EF101, APMT and A625. They all contain larger amounts of silicon and/or chromium and/or aluminum and/or nickel (see Table 1) that has been shown to influence the incubation time to breakaway as well as the corrosion behavior within the secondary regime. The current results indicate a minor difference in incubation time, see Fig. 6b_1, c_1 and d_1, while a larger difference could be observed in developing a good secondary protection. Even though the secondary corrosion resistance differs, the overall microstructure is very similar, i.e., an outward-growing iron oxide and an inward-growing more complex oxide containing all alloying elements. Since the corrosion enhancing elements (Cr, Al, Ni, and Si) mainly ends up in the inward-growing part of the scale, this indicates that the improved secondary protection may be attributed to the inward-growing oxide and is in good agreement with the investigation by Eklund et al. [48] and Persdotter et al. [43]. It may be noted that no large difference in Cl penetration/accumulation could be observed between the different alloys.

Chromium and aluminum are two of the most obvious candidates as alloying elements for improving corrosion resistance at high temperature because of their ability to form a chromia or an alumina layer, respectively. In this study, APMT (21.15 at% Cr) and A625 (24.15 at% Cr) showed improved secondary protection. The inward growing oxide scales formed by these alloys were characterized by enrichment of chromium and chromium/aluminum followed by a corresponding chromium or chromium/aluminum depletion zone beneath the scale. The results thereby indicate a "healing layer" in the bottom part of the inward growing scale even though more detailed microscopy is needed to investigate the exact phase and composition (e.g., TEM). High chromium content in the alloy has been suggested to improve corrosion resistance by preventing the internal oxidation [38]. It was reported that a chromium content of 18 wt% leads to improved corrosion resistance for FeCrAl alloys in similar environments as this study. However, it is worth noting that the amount of chromium required to improve corrosion resistance for the FeCrAl alloys also depends on the aluminum content. In the case of A625, the extent to which its high chromium content contributes to the corrosion resistance in this environment/temperature is difficult to evaluate since this alloy in addition contains a very high content of nickel. Thus, it is worth discussing the role of nickel in combination with the chromium effect.

The presence of nickel in the alloy may change the corrosion behavior in several different ways. Within the secondary regime (after breakaway oxidation) it will be present in the inward-growing spinel, which may change the diffusion properties, or as metal inclusions in combination with the miscibility gap in the Fe-Cr-O spinel system. Nickel is neither stable in the spinel oxide at low pO_2. This may also cause internal oxidation [29]. The mixed NiCr-spinel has been shown to have fast oxidation kinetics and forms at the expense of NiO [49]. The scale interpreted as spinel was enriched in Cr (about 70 at%) with less Ni (about 25 at%). Even though the Ni containing spinel may not be protective it may form a layer of separating the chromium rich oxide from the reactive alkali. Indications of this could be seen in the microstructural investigation, see Fig. 6d_1. This may promote a very good secondary protection, i.e., formation of a Cr-rich scale beneath a thicker scale (nickel oxide (NiO or spinel). The microstructure beneath the Cr rich protective scale on the bulk material showed signs of very small grain size in combination with Cr depletion and may explain the very good Cr rich oxide formed beneath the Ni rich top layer [29].

It is well known that silicon additions may improve the high temperature corrosion resistance for alloys. Studies done in KCl-rich laboratory environments [22] and field investigations, see e.g., [32] have shown that Silicon has a positive effect on the secondary protection of FeCrAl alloys. In line with these results, silicon had a positive effect on the corrosion resistance of alloy EF101. The oxide thickness measurement showed that EF101 (2.01 at% Si) exhibited better corrosion resistance than EF100 (0.5 at% Si), which has similar chemical composition except for the difference in silicon content as shown in Fig. 6a and b respectively. Both alloys formed outward-growing scales consisting of iron oxide of the same thickness while the results indicate that the inward growing layer on EF101 is thinner. The effect of Si on oxide growth after breakaway oxidation has been suggested to reduce the growth rate of the inward-growing spinel [22], which is in line with the current results. In another study, where Fe–15Cr–5Si was exposed in KCl vapor-air mixture at 650 °C for 20 h [50], it was observed that the alloy suffered less corrosion by forming an inner layer of silicon oxide beneath potassium chromate. However, in this study, no indications of a silica layer could be observed in the microstructural investigation of EF101 (2.01 at% Si).

4.3.4. Alloy/oxide microstructure – impact on secondary protection

The alloy composition has a large impact on the secondary protection in harsh environments as described above. However, the alloy microstructure may in addition influence the corrosion resistance both prior to and after breakaway oxidation. This is very important for the secondary protection as the results indicate that the main protection is given by the inward growing scale. It may in addition be noted that very similar composition gives a systematic difference in corrosion response if the overlay weld coatings are compared with the bulk materials with similar compositions. In all cases and for all exposure times the coatings provide a microstructure of the oxide with less protection than the corresponding bulk materials, compare images in Fig. 6.

The microstructural investigation of the unexposed samples and exposed samples revealed small differences in composition between the overlay weld and bulk samples but instead a very large difference in alloy grain size, compare e.g., Fig. 6b_1 and b_2. The results indicate that the supply of chromium/aluminum to the scale may play a crucial role in

improved secondary protection. All alloys showing an improved protection had a Cr-rich inner part of the scale followed by a depletion zone in the alloy below the scale/metal interface. A microstructure with a higher average diffusion ability, i.e., more alloy grain boundaries, would faster switch into this mode. This is in line with the breakdown of a protective primary scale where the supply of Cr is crucial to maintain the scale in the presence of alkali salts or H_2O [36]. Smaller alloy grains, faster transport in the bulk (BCC compared to FCC) and higher activity of Al/Cr/Si would promote an improved secondary scale. Eklund et al. [38] showed that a combination of Cr/Al may prevent internal oxidation, enabling the formation of a healing layer. It may in this context be noted that the A625 bulk material with the best secondary protection (measured oxide scale thickness of about 5 μm) formed a region of fine grains beneath the metal-oxide interface. Although the refinement process of the original alloy grains during exposure is not well established, it is believed that the formed fine grains offered faster diffusion pathways for chromium, which ultimately improved the oxidation behavior of this alloy together with the high activity of nickel in the alloy. However, the inward growing scale is thicker than a traditional primary scale (Cr_2O_3) but on the limit to investigate with SEM. More detailed investigations are therefore needed with e.g., TEM in order to investigate the actual phase of this inward-growing scale and understands more about its protectiveness in the secondary corrosion regime.

5. Conclusion

5.1. The investigation of an experimental setup for long-term exposures in the presence of KCl

In this study, a new experimental setup was developed which enables long-term corrosion investigation (up to 8000 h) in a KCl rich environment. KCl (s) was maintained on sample surfaces by ensuring low KCl evaporation rate where a low gas flow rate (0.1 cm/s) in combination with a large KCl source upstream the samples was used. The position of the samples in the furnace as well as the amount of pre-deposited KCl(s) on the samples had very limited impact on the corrosion of the reference samples.

5.2. The long-term exposures of FeCr(Ni, Al) alloys in the presence of KCl

The corrosion investigation showed that the presence of KCl(s)/KCl (g) resulted in fast breakaway oxidation for all the investigated alloys (less than 168 h). The bulk materials exhibited better corrosion resistance than the overlay weld coatings of similar composition. The measured oxide thicknesses showed that all the alloys exhibited similar corrosion trends for all the exposure durations (168 h, 500 h, 1000 h, 2000 h, and 8000 h). Oxide microstructural investigation showed that all the alloys formed duo-layered oxide scales, i.e., outward-growing, and inward-growing oxide indicating diffusion-controlled kinetics. Alloys that exhibited improved secondary protection displayed significant enrichments of Cr in the inward-growing oxide, indicating the formation of a healing layer. Besides increasing the Cr content in the alloy, the Cr enrichment in the inward-growing scale were promoted by introducing Al, Ni and Si in the alloy.

Funding

This research was funded by EC for financial support within the frame of the Horizon 2020 project "Lowering Costs by Improving Efficiencies in Biomass Fueled Boilers: New Materials and Coatings to Reduce Corrosion (BELENUS)", Grant Agreement number: 815147.

CRediT authorship contribution statement

Vicent Ssenteza: Conceptualization, Methodology, Validation, Investigation, Data curation, Writing – original draft, Writing – review & editing, Visualization. **Johan Eklund:** Conceptualization, Investigation, Writing – review & editing. **Imran Hanif:** Conceptualization, Writing – review & editing. **Jesper Liske:** Conceptualization, Writing – review & editing, Supervision. **Torbjörn Jonsson:** Conceptualization, Writing – review & editing, Supervision, Project administration.

Declaration of Competing Interest

The authors declare that they have no known competing financial interests or personal relationships that could have appeared to influence the work reported in this paper.

Data availability

Data will be made available on request.

Acknowledgements

This work was carried out within the High Temperature Corrosion Centre (HTC) at Chalmers University of Technology. The authors also acknowledge Chalmers Materials Analysis Laboratory (CMAL) where part of this research was carried out.

References

[1] W.B.A. Sharp, D.L. Singbeil, J.R. Keiser, Superheater corrosion produced by biomass fuels, in: Proceedings of the NACE – International Corrosion Conference Series, 2012, pp. 2384–2401.
[2] H.P. Nielsen, F.J. Frandsen, K. Dam-Johansen, L.L. Baxter, The implications of chlorine-associated corrosion on the operation of biomass-fired boilers, Prog. Energy Combust. Sci. 26 (2000) 283–298, https://doi.org/10.1016/S0360-1285(00)00003-4.
[3] A. Thong-On, C. Boonruang, Design of boiler welding for improvement of lifetime and cost control, Materials 9 (2016) 891, https://doi.org/10.3390/ma9110891.
[4] H.P. Michelsen, F. Frandsen, K. Dam-Johansen, O.H. Larsen, Deposition and high temperature corrosion in a 10 MW straw fired boiler, Fuel Process. Technol. 54 (1998) 95–108, https://doi.org/10.1016/S0378-3820(97)00062-3.
[5] S. Enestam, D. Bankiewicz, J. Tuiremo, K. Mäkelä, M. Hupa, Are NaCl and KCl equally corrosive on superheater materials of steam boilers? Fuel 104 (2013) 294–306, https://doi.org/10.1016/J.FUEL.2012.07.020.
[6] S.C. Cha, High temperature corrosion of superheater materials below deposited biomass ashes in biomass combusting atmospheres, Corros. Eng. 42 (2007) 50–60, https://doi.org/10.1179/174327807×159989.
[7] J. Phother-Simon, T. Jonsson, J. Liske, Continuous KCl addition in high temperature exposures of 304 L – a way to mimic a boiler environment, Corros. Sci. 167 (2020), 108511, https://doi.org/10.1016/J.CORSCI.2020.108511.
[8] J. Lehmusto, B.-J. Skrifvars, P. Yrjas, M. Hupa, High temperature oxidation of metallic chromium exposed to eight different metal chlorides, Corros. Sci. 53 (2011) 3315–3323, https://doi.org/10.1016/J.CORSCI.2011.06.007.
[9] C. Pettersson, J. Pettersson, H. Asteman, J.-E. Svensson, L.-G. Johansson, KCl-induced high temperature corrosion of the austenitic Fe–Cr–Ni alloys 304L and Sanicro 28 at 600 C, Corros. Sci. 48 (2006) 1368–1378, https://doi.org/10.1016/j.corsci.2005.05.018.
[10] N. Israelsson, K. Hellström, J.-E. Svensson, L.-G. Johansson, KCl-induced corrosion of the FeCrAl alloy Kanthal® AF at 600 °C and the effect of H2O, Oxid. Met. 83 (2015) 1–27, https://doi.org/10.1007/s11085-014-9506-3.
[11] E. Larsson, J. Liske, A. Persdotter1, T. Jonsson, J.-E. Svensson1, L.-G. Johansson, The infuence of KCl and HCl on the high-temperature oxidation of a Fe-2.25Cr-1Mo steel at 400 °C, Oxid. Met. 93 (2019) 29–52, https://doi.org/10.1007/s11085-019-09943-9.
[12] S.C. Okoro, S. Kiamehr, M. Montgomery, F.J. Frandsen, K. Pantleon, Effect of flue gas composition on deposit induced hightemperature corrosion under laboratory conditionsmimicking biomass firing. Part I: exposures in oxidizingand chlorinating atmospheres, Mater. Corros. 68 (2017) 499–514, https://doi.org/10.1002/maco.201609173.
[13] J. Eklund, J. Phother, E. Sadeghi, S. Joshi, J. Liske, High-temperature corrosion of HVAF-sprayed Ni-based coatings for boiler applications, Oxid. Met. 91 (2019) 729–747, https://doi.org/10.1007/s11085-019-09906-0.
[14] J. Eklund, A. Persdotter, I. Hanif, S. Bigdeli, T. Jonsson, Secondary corrosion protection of FeCr(Al) model alloys at 600 °C – the influence of Cr and Al after breakaway corrosion, Corros. Sci. 189 (2021), 109584, https://doi.org/10.1016/J.CORSCI.2021.109584.
[15] J. Phother-Simon, I. Hanif, J. Liske, T. Jonsson, The influence of a KCl-rich environment on the corrosion attack of 304 L: 3D FIB/SEM and TEM investigations, Corros. Sci. 183 (2021), 109315, https://doi.org/10.1016/J.CORSCI.2021.109315.

[16] N. Folkeson, T. Jonsson, M. Halvarsson, L.-G. Johansson, J.-E. Svensson, The influence of small amounts of KCl(s) on the hightemperature corrosion of a Fe-2.25Cr-1Mo steel at 400 and 5008C, Mater. Corros. 62 (2011) 606–615, https://doi.org/10.1002/maco.201005942.
[17] S. Karlsson, J. Pettersson, L.-G. Johansson, J.-E. Svensson, Alkali induced high temperature corrosion of stainless steel: the influence of NaCl, KCl and CaCl2, Oxid. Met. 78 (2012) 83–102, https://doi.org/10.1007/s11085-012-9293-7.
[18] A. Persdotter, J. Eklund, J. Liske, T. Jonsson, Beyond breakaway corrosion – influence of chromium, nickel and aluminum on corrosion of iron-based alloys at 600 °C, Corros. Sci. 177 (2020), 108961, https://doi.org/10.1016/j.corsci.2020.108961.
[19] J. Engkvist, S. Canovic, K. Hellström, A. Järdnäs, J.-E. Svensson, L.-G. Johansson, M. Olsson, M. Halvarsson, Alumina scale formation on a powder metallurgical FeCrAl alloy (Kanthal APMT) at 900–1,100 °C in dry O2 and in O2 + H2O, Oxid. Met. 73 (2010) 233–253, https://doi.org/10.1007/s11085-009-9177-7.
[20] N. Israelsson, K.A. Unocic, K. Hellström, T. Jonsson, M. Norell, J.-E. Svensson, L.-G. Johansson, A microstructural and kinetic investigation of the KCl-induced corrosion of an FeCrAl alloy at 600 °C, Oxid. Met. 84 (2015) 105–127, https://doi.org/10.1007/s11085-015-9546-3.
[21] Y. Alipour, P. Henderson, Corrosion of furnace wall materials in waste-wood fired power plant, Corros. Eng. Sci. Technol. 50 (2015) 355–363, https://doi.org/10.1179/1743278214Y.0000000228.
[22] J. Eklund, B. Jönsson, A. Persdotter, J. Liske, J.-E. Svensson, T. Jonsson, The influence of silicon on the corrosion properties of FeCrAl model alloys in oxidizing environments at 600 °C, Corros. Sci. 144 (2018) 266–276, https://doi.org/10.1016/j.corsci.2018.09.004.
[23] J. Eklund, High Temperature Corrosion of FeCrAl Alloys in Biomass- and Wastefired Boilers. The Influence of Alloying Elements in Prediction and Mitigation of Corrosion in Harsh Environments (Thesis for the Degree of Doctor of Philosophy), Chalmers University of Technology, 2020. ⟨https://research.chalmers.se/publication/521876/file/521876_Fulltext.pdf⟩.
[24] J. Sui, J. Lehmusto, M. Bergelin, M. Hupa, The effects of KCl, NaCl and K2CO3 on the high-temperature oxidation onset of sanicro 28 steel, Oxid. Met. 85 (2016) 565–598, https://doi.org/10.1007/s11085-016-9613-4.
[25] M. Subanović, J. Pirón, A. Gauss, M. Jarrar, A. Schneider, Super VM12- a new 12% CR boiler steel, in: J. Shingledecker, M. Takeyama (Eds.), Proceedings of the Joint EPRI – 123HiMAT International Conference on Advances in High-Temperature Materials, ASM International, Nagasaki, Japan, 2019, pp. 205–216.
[26] H.P. Nielsen, L.L. Baxter, G. Sclippab, C. Morey, F.J. Frandsen, K. Dam-Johansen, Deposition of potassium salts on heat transfer surfaces in straw-fired boilers: a pilot-scale study, Fuel 79 (2000) 131–139, https://doi.org/10.1016/S0016-2361(99)00090-3.
[27] S. Karlsson, E. Larsson, T. Jonsson, J. Liske, J.-E. Svensson, A laboratory study of the in situ sulfation of alkali chloride rich deposits: corrosion perspective, Energy Fuels 30 (2016) 7256–7267, https://doi.org/10.1021/acs.energyfuels.6b00372.
[28] Y.C. Malede, J.P. Simon, T. Jonsson, M. Montgomery, K.V. Dahl, J. Hald, KCl-induced corrosion of Ni-based alloys containing 35–45 wt% Cr, Mater. Corros. 70 (2019) 1486–1506, https://doi.org/10.1002/maco.201810658.
[29] T. Jonsson, H. Larsson, S. Karlsson, H. Hooshyar, M. Sattari, J. Liske, J.-E. Svensson, L.-G. Johansson, High-temperature oxidation of FeCr(Ni) alloys: the behaviour after breakaway, Oxid. Met. 87 (2017) 333–341, https://doi.org/10.1007/s11085-017-9731-7.
[30] M. Montgomery, A. Karlsson, O.H. Larsen, Field Test Corrosion Experiments in Denmark with Biomass Fuels Part 1: Straw-firing Korrosionsfeldversuche in Da È nemark mit Brennstoffen aus Biomasse Teil 1: Strohfeuerung, n.d.
[31] P. Andersson, M. Norell, Field test of superheater corrosion in a CFB waste boiler: part II – scale formation characteristics, Mater. Corros. 56 (2005) 550–560, https://doi.org/10.1002/maco.200403853.
[32] J. Eklund, B. Paz, Maria Dolores Jönsson, J. Liske, J.-E. Svensson, T. Jonsson, Field exposure of FeCrAl model alloys in a waste-fired boiler at 600°C: The influence of Cr and Si on the corrosion behaviour, Mater. Corros. 70 (2019) 1476–1485.
[33] Y.C. Malede, K.V. Dahl, M. Montgomery, F.B. Grumsen, J. Hald, Effect of service exposure on KCl corrosion attack of AISI 347H FG steel, J. Mater. Sci. 54 (2019) 13787–13809, https://doi.org/10.1007/s10853-019-03863-4.
[34] Y.S. Li, M. Spiegel, S. Shimada, Corrosion behaviour of various model alloys with NaCl–KCl coating, Mater. Chem. Phys. 93 (2005) 217–223, https://doi.org/10.1016/J.MATCHEMPHYS.2005.03.015.
[35] T. Jonsson, J. Froitzheim, J. Pettersson, J.-E. Svensson, L.-G. Johansson, M. Halvarsson, The influence of KCl on the corrosion of an austenitic stainless steel (304L) in oxidizing humid conditions at 600°C: a microstructural study, Oxid. Met. 72 (2009) 213–239, https://doi.org/10.1007/s11085-009-9156-z.
[36] J. Pettersson, H. Asteman, J.E. Svensson, L.G. Johansson, KCl induced corrosion of a 304-type austenitic stainless steel at 600°C; the role of potassium, Oxid. Met. 64 (2005) 23–41, https://doi.org/10.1007/s11085-005-5704-3.
[37] J. Lehmusto, M. Olin, J. Viljanen, J. Kalliokoski, F. Mylläri, J. Toivonen, M. Dal Maso, L. Hupa, Detection of gaseous species during KCl-induced high-temperature corrosion by the means of CPFAAS and CI-APi-TOF, Mater. Corros. 71 (2020) 222–231, https://doi.org/10.1002/maco.201910964.
[38] J. Eklund, I. Hanif, S. Bigdeli, T. Jonsson, High temperature corrosion behavior of FeCrAlSi model alloys in the presence of water vapor and KCl at 600 °C – the influence of Cr content, Corros. Sci. 198 (2022), 110114, https://doi.org/10.1016/J.CORSCI.2022.110114.
[39] P.C. Nordine, P.W. Gilles, Undersaturation dependence of the evaporation rate of potassium chloride, J. Chem. Phys. 74 (1981) 5242, https://doi.org/10.1063/1.441734.
[40] B. Pujilaksono, T. Jonsson, H. Heidari, M. Halvarsson, J.-E. Svensson, L.-G. Johansson, Oxidation of binary FeCr alloys (Fe–2.25Cr, Fe–10Cr, Fe–18Cr and Fe–25Cr) in O2 and in O2 + H2O environment at 600 °C, Oxid. Met. 75 (2011) 183–207, https://doi.org/10.1007/s11085-010-9229-z.
[41] H. Asteman, J.-E. Svensson, L.-G. Johansson, Evidence for chromium evaporation influencing the oxidation of 304L: the effect of temperature and flow rate, Oxid. Met. 57 (2002) 193–216, https://doi.org/10.1023/A:1014877600235.
[42] M. Halvarsson, J.E. Tang, H. Asteman, J.-E. Svensson, L.-G. Johansson, Microstructural investigation of the breakdown of the protective oxide scale on a 304 steel in the presence of oxygen and water vapour at 600 °C, Corros. Sci. 48 (2006) 2014–2035, https://doi.org/10.1016/j.corsci.2005.08.012.
[43] A. Persdotter, J. Eklund, J. Liske, T. Jonsson, Beyond breakaway corrosion – influence of chromium, nickel and aluminum on corrosion of iron-based alloys at 600 °C, Corros. Sci. 177 (2020), 108961, https://doi.org/10.1016/j.corsci.2020.108961.
[44] H.J. Grabke, E. Reese, M. Spiegel, The effects of chlorides, hydrogen chloride, and sulfur dioxide in the oxidation of steels below deposits, Corros. Sci. 37 (1995) 1023–1043, https://doi.org/10.1016/0010-938X(95)00011-8.
[45] N. Folkeson, L.-G. Johansson, J.-E. Svensson, Initial stages of the HCl-induced high-temperature corrosion of alloy 310, J. Electrochem Soc. 154 (2007) C515, https://doi.org/10.1149/1.2754174.
[46] J. Töpfer, S. Aggarwal, R. Dieckmann, Point defects and cation tracer diffusion in (CrxFe1 − x)3 − δO4 spinels, Solid State Ion. 81 (1995) 251–266, https://doi.org/10.1016/0167-2738(95)00190-H.
[47] T. Jonsson, B. Pujilaksono, A. Fuchs, J.E. Svensson, L.G. Johansson, M. Halvarsson, The influence of H2O on iron oxidation at 600°C: a microstructural study, Mater. Sci. Forum 595–598 (2008) 1005–1012, https://doi.org/10.4028/www.scientific.net/MSF.595-598.1005.
[48] J. Eklund, A. Persdotter, I. Hanif, S. Bigdeli, T. Jonsson, Secondary corrosion protection of FeCr(Al) model alloys at 600 °C – the influence of Cr and Al after breakaway corrosion, Corros. Sci. 189 (2021), https://doi.org/10.1016/J.CORSCI.2021.109584.
[49] D.L. Douglass, J.S. Armijo, The Effect of Silicon and Manganese on the Oxidation Mechanism of Ni-20Cr, 1970.
[50] Y.S. Li, Y. Niu, M. Spiegel, High temperature interaction of Al/Si-modified Fe–Cr alloys with KCl, Corros. Sci. 49 (2007) 1799–1815, https://doi.org/10.1016/J.CORSCI.2006.10.019.